CMS Physics Analysis Summary

Contact: cms-pag-conveners-top@cern.ch 2012/07/13

Measurement of Spin Correlations in $t\bar{t}$ events in the dilepton channels in pp collisions at $\sqrt{s} = 7$ TeV

The CMS Collaboration

Abstract

We present a measurement of the top spin correlation in $t\bar{t}$ production in the dilepton channels in pp collisions at $\sqrt{s}$ =7 TeV. The data sample used for the measurement corresponds to an integrated luminosity of 5.0$\pm$0.1 fb^{-1} collected with the CMS detector at the LHC. The measurement is performed in events with two leptons (electrons or muons) in the final state, and at least two jets where at least one is identified as originating from a b-quark. In addition the presence of missing transverse energy is required. The spin correlation in $t\bar{t}$ events is extracted from a fit to the angular distribution between the two selected leptons. In the helicity basis, the correlation coefficient is found to be 0.24$\pm$0.02(stat.)$\pm$0.08(syst.). The spin correlation is also investigated through other variables and for different $t\bar{t}$ invariant masses. All measurements are found to be in agreement with the standard model predictions.

1 Introduction

At the LHC, top quarks are produced abundantly, mainly in pairs by gluon fusion. The top quark mass has been measured to be 172.9 $\pm$ 0.6 $\pm$ 0.9 GeV/c^2 [1] and the width of the top quark is found to be $\Gamma_t = 2.0^{+0.7}_{-0.6}$ GeV[1]. This implies a lifetime much shorter than the hadronization time-scale, m_t/Λ^2_{QCD}. Therefore, the spin of the top quark at production is transferred to its decay products and can be accessed by the distribution of angular observables. The study of the spin correlation of the $t\bar{t}$ pairs then become possible [2]. The investigation of spin correlation in the $t\bar{t}$ system probes the bare quark at production, and by this the top pair production processes and perturbative QCD. At the LHC, for low invariant mass of the $t\bar{t}$ pair, the production is dominated by the fusion of like-helicity gluon pairs, resulting in top pairs with aligned orientations ($\uparrow\uparrow$ or $\downarrow\downarrow$) of top and anti-top spins. At higher invariant masses, the dominant production switches to unlike-helicity gluons, producing $t\bar{t}$ pairs in anti-aligned orientations ($\uparrow\downarrow$ or $\downarrow\uparrow$), which give identical configurations than the ones produced by $q\bar{q}$ annihilation at the Tevatron [3]. In the dileptonic decay through $t\bar{t} \rightarrow l^+\nu l^-\bar{\nu}b\bar{b}$, the charged leptons are correlated in azimuthal angle ($\Delta\phi_{l^+l^-}$) in the laboratory frame [3] and can be measured precisely by the LHC experiments without reconstructing the full event kinematics. CDF and D0 measured the strength of the $t\bar{t}$ spin correlation to be in agreement with the standard model (SM) expectation using template fit methods to angular distributions[4–6]. The ATLAS experiment reported a measurement of the spin correlation using the $\Delta\phi_{l^+l^-}$ distributions and found it to be in agreement with next-to-leading order SM predictions [7].

This analysis uses data corresponding to an integrated luminosity of 5 fb^{-1} of proton-proton collisions at $\sqrt{s}$ = 7 TeV, provided by the LHC and recorded by the CMS detector [8]. The measurement of the spin correlation in $t\bar{t}$ events is compared to the SM expectation.

In addition to the measurement of the spin correlation coefficient, performed using the $\Delta\phi_{l^+l^-}$ distribution, we present the measurement of asymmetries related to the spin correlation.

The description of the data-sets and simulated samples is given in Sec. 2. The baseline event selection is presented in Sec. 3. A short presentation of the data-driven techniques used to estimate the background contamination can be found in Sec. 4, while the description of the systematic effects are discussed in Sec. 5. The measurements are presented in Sec. 6, followed by our conclusion in Sec. 7.

2 Simulation of signal and backgrounds

The $t\bar{t}$ signal events are simulated with either MC@NLO [9] or POWHEG [10] Monte Carlo (MC) packages. Four samples are produced with and without spin correlation through MC@NLO. Parton showering and hadronization of the events is simulated by HERWIG6 for MC@NLO and by PYTHIA [11] for POWHEG. The simulated $t\bar{t}$ signal events produced with and without spin correlation are processed with the fast detector simulation [12] (FastSim), while all other simulated events are processed with the GEANT4-based [13] CMS detector simulation (FullSim). All events are reconstructed using the same software as used for collision data. The samples processed with FastSim detector simulation are validated by comparing distributions obtained from events processed with full detector simulation. The kinematic variables of muons and electrons, and the invariant lepton pair masses, the missing transverse energy and the b-tagging information are compatible within uncertainties. Some discrepancies between FastSim and FullSim are observed on the multiplicity of selected jets. These differences are treated as a systematic uncertainty in the analysis.

For the signal samples, a top quark mass of m_{top} =172.5 GeV/c^2 is assumed. Additional samples with and without spin correlation and an assumed top mass of 170 and 175 GeV/c^2 are produced with MC@NLO for systematic uncertainty calculations. Moreover, simulations of the $t\bar{t}$ signal sample with an increased and decreased factorisation and renormalisation scale are produced using MC@NLO with HERWIG6. These samples are also generated with and without spin correlation to estimate systematic uncertainties on modelling of signal $t\bar{t}$ events and of the showering.

The main sources of background are the events from W/Z+jets in which the vector boson decays leptonically, and single top quark. The electro-weak production of single top quarks in the tW channel is simulated using POWHEG or PYTHIA. The corresponding cross-section of 15.7$\pm$0.4 pb is used in this analysis. The W/Z+jets events are processed using MADGRAPH [14], with up to four jets where the jet flavor is inclusive. The corresponding NNLO cross sections, calculated by the FEWZ program [15], are 31.3$\pm$1.6 nb and 15.0$\pm$0.77 nb, respectively. The diboson processes, WW, WZ, ZZ , are simulated using PYTHIA or MADGRAPH. The corresponding cross sections used in this analysis are 47.0$\pm$1.7 pb, 18.2$\pm$0.7 pb and 7.7$\pm$0.2 pb, respectively for the WW, WZ and ZZ events.

Among the simulated backgrounds, only the predictions for the diboson and single top quark backgrounds are used in the analysis. The normalisations of all other backgrounds are estimated from data, as discussed in Section 4.

Pileup effects are modelled in the simulation by mixing simulated minimum bias events, to the simulated events with an event multiplicities which corresponds to the pileup profile of pp collisions at the LHC.

3 Event selection

The baseline event selection applied to preform the measurements, as well as the reconstruction algorithms of objects, are presented in this section. Selection requirements which are specific to a measurement are discussed in Sec.6.1 and 6.2.

Events in data are collected using dilepton triggers that require the presence of at least two muons, two electrons or one electron and one muon in the events, with various threshold on the transverse momentum (p_T) of the leptons. The efficiency of the trigger selection in data was estimated using cross-triggers, as discussed in Ref. [16] and the trigger efficiency in the simulation is corrected with the corresponding data-to-simulation scale factors of 0.977$\pm$0.015, 0.962$\pm$0.016 and 1.008$\pm$0.009 for the $\mu^+\mu^-$, e^+e^- and $e^\pm\mu^\mp$ channels respectively.

After requiring the presence of a primary vertex in the events, with a distance to the centre of the detector $<$ 24 cm along the axis of the beam line and within 2 cm in the transverse plan, at least two reconstructed leptons with opposite electric charge in the event are required. The electrons are reconstructed by associating tracks from the inner tracker with calorimetric clusters in the electromagnetic calorimeter. Muons are reconstructed by matching tracks from the outer muon detector to the tracks reconstructed by the inner tracker. To reject jets or hadrons wrongly reconstructed as leptons, specific lepton identification criteria are applied on both lepton flavor [17, 18].

The leptons are required to have $p_T > 20$ GeV and to satisfy $|\eta| < 2.1$ and $|\eta| < 2.5$ for electrons and muons respectively. The track of the lepton candidates are required to have an origin compatible with the primary vertex position, and further quality requirements are applied [16]. Leptons coming from W decays (excluding the τ) are expected to be isolated from any other

particles. Thus, lepton candidates are required to be isolated from other activities in the tracker, or in the calorimeter. A cone of $\Delta R = 0.3$ (with $\Delta R = \sqrt{\Delta\phi^2 + \Delta\eta^2}$), constructed around the lepton directions, is used to collect the transverse energy deposited close to the lepton, excluding the contribution of the lepton candidate. The energy deposition in the cone is estimated using Particle-Flow (PF) candidates [19], excluding PF candidates associated to pileup events. The ratio of the sum of the transverse energy deposited within the cone to the p_T of the lepton candidate defines the lepton isolation I_{rel}. The lepton candidates are rejected if they do not satisfy $I_{rel} < 0.17$ and $I_{rel} < 0.20$, for electrons and muons respectively.

Lepton reconstruction efficiencies are close to 100% [17, 18]. The lepton selection efficiencies are estimated with a tag&probe method [16, 20] as a function of p_T and η of the leptons. Comparing the lepton selection efficiencies in data and the simulation, inclusive data-to-simulation scale factors of 0.997±0.005, 0.995±0.005 and 0.994±0.005 are found for $t\bar{t}$ signal events, accounting for the p_T and η dependence of the scale factors. In order to reject Drell-Yan events, the dilepton invariant mass is required to be outside the range [76, 106] GeV.

The jets are reconstructed from PF candidates [19] using an anti-k_T algorithm [21] with a cone size of 0.5. The charged particles coming from pileup events are rejected by requiring the PF candidates to be associated to the main primary vertex. The neutral component from pileup events is accounted using the so called area-based procedure described in Ref. [22, 23]. Jet energy corrections are used. They rely on MC simulations and on studies performed with two-jets and photon+jet events in data [24].

B jets from top decays are identified as originating from the hadronization of a b-quark using the "Combined Secondary Vertex" (CSV) algorithm [25]. The performance of the b-tagging selection is estimated using QCD multi-jets events as described in [26]. As an example, the loose working point of CSV corresponds to a b-tagging efficiency of 80-85% for a mis-tagging rate of about 10%, as estimated from the simulation.

Because of the presence of escaping neutrinos in $t\bar{t}$ signal events, the transverse missing energy $\not{E}_T$ can either be used to reject backgrounds like $Z/\gamma^\star$ events or for the reconstruction of $t\bar{t}$ events. The $\not{E}_T$ vector is defined as $\not{E}_T = -\sum_i p_T^i$, where the sum is done over the PF candidates, excluding those coming from pileup events [27]. The $\not{E}_T$ is then the norm of $\not{E}_T$ vector.

The thresholds applied on the b-tagging discriminator and on the $\not{E}_T$ are discussed in Secs.6.1 and 6.2.

4 Background estimates

The contamination from two different kinds of backgrounds is estimated from data. The first is the production of DY lepton pair events. The second is the production of W-like and QCD multijet events that have one or two non-prompt leptons, not coming from W or $Z/\gamma^\star$ decays.

The DY background is dominant in the e^+e and $\mu^+\mu^-$ channels. It is estimated from the number of events in data inside the dilepton invariant mass window of 76 GeV/c^2 $< m_{\ell\ell} <$ 106 GeV/c^2, scaled by the ratio of events that fail and pass this selection.

The non-prompt lepton backgrounds are estimated by first defining a looser definition of lepton isolation. Then different dilepton samples are constructed. The first (loose) sample contain events that has two loose leptons, the second (medium) sample contain events that has at least one tight lepton, and the third (tight) sample contain events that has two tight leptons. By introducing the probability for prompt lepton and non-prompt lepton to pass the loose and

tight isolation criteria, one can construct a system of linear equations with the number of events with two prompt-lepton ($t\bar{t}$ and DY) and events with one or two prompt leptons as unknowns. Solving this system of linear equations yields the expected background from W-like and QCD multijet events [16]. This method is known as the matrix method in the literature [28], or Barlow's event reweighting method [29]. Another similar method [30], based on the rate of non-prompt leptons, is used in Sec. 6.2.

A more detailed description of the methods used to estimate the backgrounds from data can be found in Refs. [16, 30, 31]. Other background contamination, coming from single top quark events and diboson events, is estimated from simulation.

5 Systematic uncertainties

Various systematic effects are affecting the measurements. Some of them are related to detector effects, others are related to the modelling of $t\bar{t}$ signal events. The main sources of systematic uncertainties are listed below.

The experimental systematic effects are :

- **Lepton selection** : uncertainties on the dilepton trigger and lepton selection (isolation and identification) affect the normalisation of signal and background events, but also influence the shapes of the angular distributions of leptons. The corresponding effects on the measurements are estimated by changing the scale factors within their uncertainties.
- **Lepton energy scale** : the uncertainty on lepton energy scale, which affects mainly the p_T distribution of leptons, is of 0.5% for electrons and negligible for muons, as estimated from comparisons between data and simulated Z events. The corresponding systematic uncertainties on the measurements are estimated by performing the fit with the energy scale of electrons varied by $\pm$ 0.5%.
- **Jet energy scale and jet energy resolution** : the uncertainty from the jet energy scale (JES) correction is first estimated by variation the JES of jets within their uncertainties, with the proper propagation to the $\not{E}_T$. The jet energy resolution (JER) is estimated similarly, but by varying the JER by 5 to 10%, depending on the η of the jet.
- **Background events** : the uncertainty on the normalisation of backgrounds is considered by varying the background by 100%.
- **Pileup (PU) modelling** : the uncertainty of 8% on the proton-proton cross section at the LHC energy of 7 TeV influence the pileup modelling and is used to estimate the corresponding systematics.
- **FastSim vs FullSim** : the measurement presented in Sec.6.1 use FastSim. The observed discrepancies between FastSim and FullSim, manifesting itself mainly in the jet multiplicity distribution, are accounting be comparing the $\Delta\phi_{l^+l^-}$ distributions between FastSim and FullSim. As the measurement presented in Sec. 6.2 does not use FastSim samples, it is not affected by this systematic.

The systematic uncertainties related to the modelling of $t\bar{t}$ signal events are :

- **Factorisation and renormalisation scales** : the uncertainty related to the factorisation and renormalisation scales is estimated by producing MC@NLO samples with factorisation and renormalisation scales divided and multiplied by a factor of 2 with

respect to their initial values, the default scale squared being :

$$\mu_0^2 \;=\; \frac{1}{2}(m_{top}^2 + p_T(top) + m_{antitop}^2 + p_T anti(top). \tag{1}$$

- **Spin correlation and τ decay** : as the decays of τ are performed by either PYTHIA or HERWIG, the effect of spin correlation is not properly propagated to the decay products of the τ. As about 15% of the dilepton $t\bar{t}$ signal events are containing at least one electron or muon from τ decay, this introduce a systematic effect. The corresponding uncertainty is estimated by comparing simulated events with and without excluding events containing at least one lepton from τ decay.
- **Top quark mass**: the uncertainty on the top quark mass is estimated using $t\bar{t}$ signal events with generated with different top masses, as discussed in Sec. 2, assuming a uncertainty on the top mass of 2.5 GeV around $m_t = 172.5$ GeV.
- **PDF** : the uncertainty related to PDF are estimated by using the so called brut force formula, as described in Ref. [32].

6 Measurement of spin correlation in $t\bar{t}$ events

6.1 Spin correlation using $\Delta\phi$ distributions

The angular difference in the azimuthal plane between the two leptons coming from the W decays in $t\bar{t}$ events ($\Delta\phi_{l^+l^-} = |\phi_{l^+} - \phi_{l^-}|$) is sensitive to the spin correlation of the two top quarks. The spin correlation is estimated by fitting the $\Delta\phi_{l^+l^-}$ distribution observed in data.

The fit is performed using a data-set constituted of events passing the baseline selection described in Sec.3. The events are also required to have a dilepton invariant mass above 20 GeV for the three channels and a $\not\!\!E_T$ above 40 GeV for the e^+e^- and $\mu^+\mu^-$ channels only. In addition, at least one of the selected jet should pass the loose working point of the CSV b-tagging algorithm.

A comparison of the $\Delta\phi_{l^+l^-}$ distributions in $t\bar{t}$ events simulated with MC@NLO with and without spin correlation can be seen in Fig.1.

The strength of the spin correlation can be measured through the spin correlation coefficient, defined as the difference between the number of $t\bar{t}$ events with spin orientation of top quarks aligned and anti-aligned, divided by the total number of $t\bar{t}$ events, namely :

$$A = \frac{N(\uparrow\uparrow) + N(\downarrow\downarrow) - N(\downarrow\uparrow) - N(\uparrow\downarrow)}{N(\uparrow\uparrow) + N(\downarrow\downarrow) + N(\downarrow\uparrow) + N(\uparrow\downarrow)}, \tag{2}$$

where the arrows are referring to the orientation of the spin of the top and anti-top quarks with respect to the chosen quantisation axis.

The spin correlation coefficient is estimated from the $\Delta\phi_{l^+l^-}$ distribution observed in data, by means of a template fit. Three different templates are considered: the $\Delta\phi_{l^+l^-}$ distributions from simulated $t\bar{t}$ events with and without spin correlation between the top quarks, and a $\Delta\phi_{l^+l^-}$ distribution which describe the background events.

A binned likelihood fit method is used, as implemented in RooFit [33], to perform a simultaneous fit of the e^+e^-, $\mu^+\mu^-$ and $e^\pm\mu^\mp$ channels. All the events are fitted together in a single likelihood fit, but different templates are used according to the decay channel (e^+e^-, $\mu^+\mu^-$

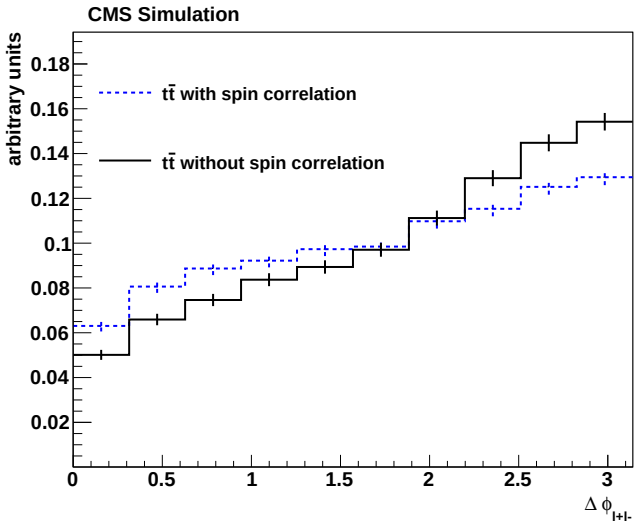

Figure 1: $\Delta\phi_{l^+l^-}$ distributions after the event selection for $t\bar{t}$ signal events with spin correlation compatible with the SM, and without spin correlation. The e^+e^-, $\mu^+\mu^-$ and $e^\pm\mu^\mp$ channels are summed.

and $e^\pm\mu^\mp$). A single template per decay channel is used to described the backgrounds events, where the templates for each background process are summed. The templates are derived from the simulation, and weighted by the data-driven estimates for the $Z/\gamma^\star$ and non-prompt lepton background, and the prediction from the simulation for the single top quark and the diboson backgrounds.

The templates for $t\bar{t}$ signal events are derived from the MC@NLO events produced with and without spin correlation. The number of $t\bar{t}$ signal events in each decay channel are parameters of the fit, as well as the fraction f of events with spin correlation. The parameter f is the same for the three channels.

The bias of this method is determined using ensembles of pseudo-experiments based on the expected numbers of signal and background events, for different hypotheses of spin correlation f from -1 to 2. A fraction > 1 would indicate a measured spin correlation stronger than the prediction of the MC@NLO generator, while $f < 0$ would corresponds to anti-correlation of top and anti-top spins. No bias is observed on the measured fraction. The width of the pull distribution is within 10% of unity over the whole range, and the average pull width is used to rescale the statistical uncertainty.

The result of the fit performed on data is shown in Fig 2, combining the e^+e^-, $\mu^+\mu^-$ and $e^\pm\mu^\mp$ channels. The number of $t\bar{t}$ signal is measured to be 1717.7 ± 44.3 in the e^+e^- channel, 2132.0 ± 50.0 in the $\mu^+\mu^-$ channel and 6351.2 ± 84.5 in the $e^\pm\mu^\mp$ channel. The fraction of spin correlation f is measured to be 0.74 ± 0.08. The uncertainties are statistical only. The total number of background events, dominated by the $Z/\gamma^\star$ processes, are 241.4 ± 120.7 , 349.2 ± 174.8 and 742.7 ± 371.4 for the e^+e^-, $\mu^+\mu^-$ and $e^\pm\mu^\mp$ channels respectively.

The systematic uncertainties are estimated using pseudo-experiments created from simulated events, modified according to the systematic effects under study. The various sources of systematic effects are discussed in Sec. 5. For each source, pseudo-experiments are generated from simulated event samples for which the relevant parameters are varied, and fit with the templates derived with the nominal parameters. The average variation of the spin correla-

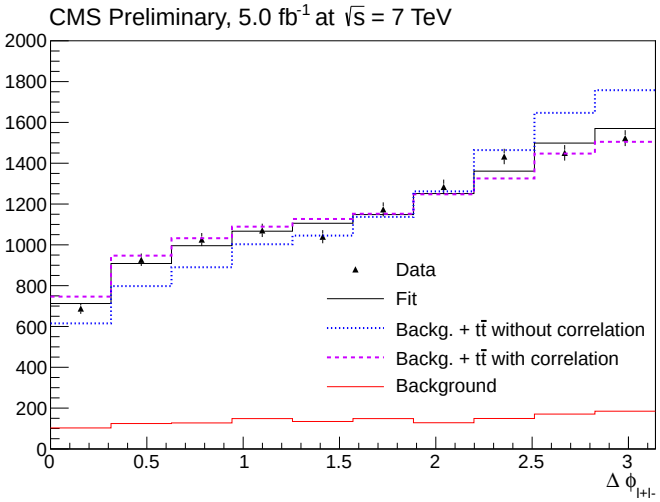

Figure 2: Result of the fit (solid line) performed on data (triangles) after the combination of the three channels. The data are also compared to the $\Delta\phi_{l^+l^-}$ distribution of $t\bar{t}$ events with and without spin correlation. The background components are included in the plot.

tion is used to estimate the systematic uncertainty. The effects of the systematic sources on the measurement of f are presented in Tab.1. The resulting measured value of f is $0.74 \pm 0.08(\text{stat.}) \pm 0.24(\text{syst.})$.

uncertainty Δf	absolute	relative (%)
statistic uncertainty	0.08	11%
MC stat uncertainty	0.07	9%
	experimental	
Lepton selection	0.01	1%
Lepton energy scale	0.01	1%
JES/JER	0.02	3%
all backgrounds	0.07	9%
PU	0.02	3%
b-tagging	0.01	1%
	$t\bar{t}$ modelling	
FastSim vs FullSim	0.06	8%
Fact. and renorm. scales	0.15	20%
τ decay	0.12	16%
top mass	0.02	3%
PDF	0.07	9%

Table 1: Uncertainty on the fraction of events with spin correlation Δf, as predicted by the fit.

Considering the top spin correlation used in the MC@NLO simulation, A^{simu}, the measured spin correlation coefficient is $f \times A^{simu}$. The spin correlation coefficient from MC@NLO $t\bar{t}$ signal events, in the helicity basis, A^{simu}_{hel}, is estimated at matrix element level and is found to be 0.33. This value of the spin correlation coefficient is close to the standard model prediction (NLO calculation) of $A^{SM}_{hel} = 0.31$ from Ref.[34], while the measurement yields a spin correlation coefficient of $A^{meas}_{hel} = 0.24 \pm 0.02(\text{stat.}) \pm 0.08(\text{syst.})$.

6.2 Measurement of asymmetries related to the spin correlation

In addition to the measurement of the spin correlation coefficient, we also present a measurement of the following asymmetry variables:

$$A_{\Delta\phi} = \frac{N(\Delta\phi_{l^+l^-} < \pi/2) - N(\Delta\phi_{l^+l^-} > \pi/2)}{N(\Delta\phi_{l^+l^-} < \pi/2) + N(\Delta\phi_{l^+l^-} > \pi/2)},$$

where $\Delta\phi_{l^+l^-}$ is the azimuthal angle between the two leptons as defined in the previous section; and

$$A_{c1c2} = \frac{N(\cos(\theta_l^+) \times \cos(\theta_l^-) > 0) - N(\cos(\theta_l^+) \times \cos(\theta_l^-) < 0)}{N(\cos(\theta_l^+) \times \cos(\theta_l^-) > 0) + N(\cos(\theta_l^+) \times \cos(\theta_l^-) < 0)},$$

where $\theta_l^{\pm}$ is the production angle of the lepton with respect to the direction of the parent top or anti-top in the $t\bar{t}$ rest frame. This quantity gives a direct measure of the spin correlation.

These variables are sensitive to $t\bar{t}$ spin correlation and can be used to study the different models which could explain the large deviation of the $t\bar{t}$ forward-backward asymmetry observed at the Tevatron [35, 36], as discussed in Ref. [37].

In addition to the baseline event selection described in Sec. 3, at least one of the selected jets has to be identified as a b-jet using the medium working point of the CSV tagger. The $\not{E}_T$ in the event is also required to larger than 30 GeV in all dilepton channels. Finally, the dilepton invariant masses are required to be greater than 12 GeV and the pseudo-rapidity selection of muons is changed to $|\eta| < 2.4$. This results in a tighter selection compared to the one presented in Sec. 6.1, with more than 90% of the selected events being $t\bar{t}$ signal events, as predicted by the simulation.

The determination of the background contamination using data, described in Sec. 4, is used to cross-check the predictions of the simulation, and consistency is observed within the uncertainties. Therefore, the background predictions are taken from simulation, while the systematic uncertainties considered are those from the background estimations done using data. The yield of simulated $t\bar{t}$ signal events is normalized such that the total simulated yield matches the number of events in data.

The observable $A_{\Delta\phi}$ is determined using only the reconstructed leptons, but the observable A_{c1c2} requires the reconstruction of the entire $t\bar{t}$ system. The presence of two neutrinos from W boson decays as well as the ambiguity in the association of each lepton to the b-jet from the same top decay, make the event reconstruction in $t\bar{t}$ dilepton events complex. Events are reconstructed using the Matrix Weighting Technique (MWT) [38], where each event is reconstructed assuming a top quark mass in the range 100-300 GeV. For each assumed mass, the $t\bar{t}$ kinematics are reconstructed and weights are calculated for each possible solution, with larger weights representing higher probabilities to have reconstructed the correct $t\bar{t}$ kinematics. The M_t hypothesis and the $t\bar{t}$ kinematics are then taken from the solution with largest weight. No solutions are found for approximately 17% of events, both in data and in the simulation, and such events are not used in the measurement of A_{c1c2}.

New physics is expected to be more prominent at high $t\bar{t}$ invariant mass, $M_{t\bar{t}}$ [37]. We thus compare the data to the simulation for $A_{\Delta\phi}$ and A_{c1c2} before and after requiring $M_{t\bar{t}} > 450$ GeV. The results are shown in Fig. 3 and 4, and the corresponding asymmetries are summarized in Tab. 2. Agreement between the data and the simulation is observed without any $M_{t\bar{t}}$ requirement as well as for $M_{t\bar{t}} > 450$ GeV.

Table 2: Reconstructed and simulated asymmetries, without any $M_{t\bar{t}}$ requirement and in the region where $M_{t\bar{t}} > 450$ GeV. Uncertainties are statistical only.

Reconstructed asymmetries	Data	Simulation
$A_{\Delta\phi}$, inclusive region	-0.158 ± 0.010	-0.171 ± 0.002
A_{c1c2}, inclusive region	-0.062 ± 0.011	-0.087 ± 0.002
$A_{\Delta\phi}$, $M_{t\bar{t}} > 450$ GeV	-0.378 ± 0.019	-0.384 ± 0.003
A_{c1c2}, $M_{t\bar{t}} > 450$ GeV	-0.019 ± 0.016	-0.044 ± 0.003

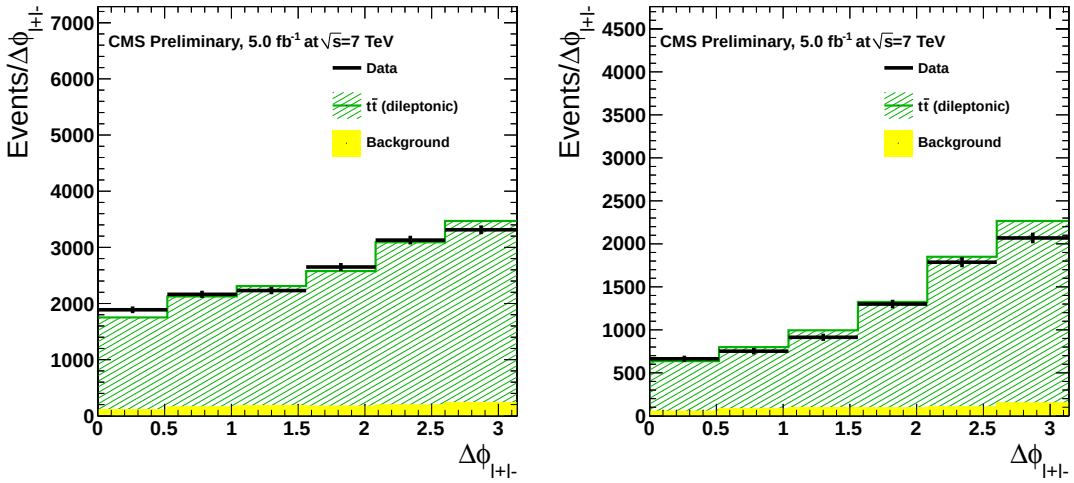

Figure 3: Distributions of $\Delta\phi_{l^+l^-}$, without $M_{t\bar{t}}$ requirement (left) and for events satisfying $M_{t\bar{t}} > 450$ GeV (right). The $t\bar{t}$ signal component is taken from the POWHEG-PYTHIA $t\bar{t}$ sample. The $t\bar{t}$ signal yields are normalized to match the data.

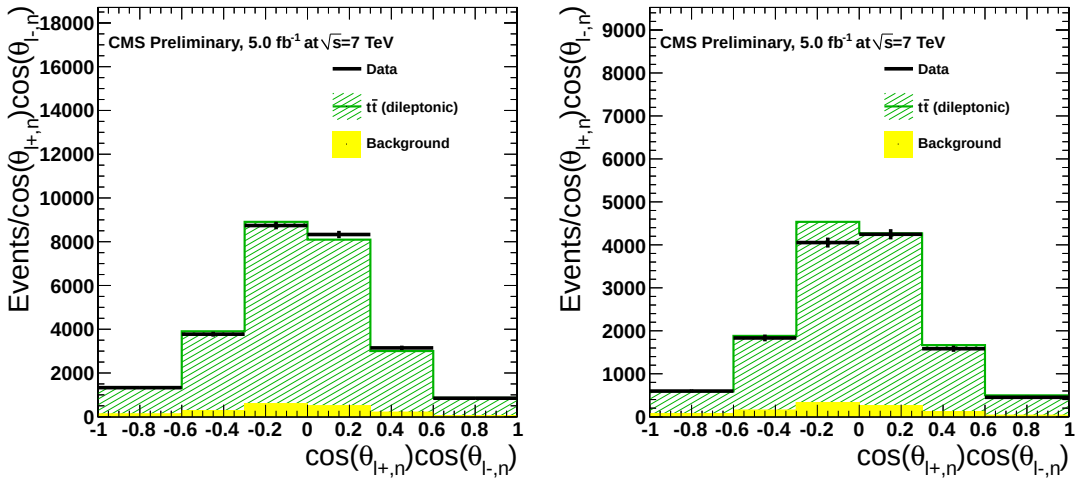

Figure 4: Distributions of $\cos(\theta_l^+) \times \cos(\theta_l^-)$, without $M_{t\bar{t}}$ requirement (left) and for events satisfying $M_{t\bar{t}} > 450$ GeV (right). The $t\bar{t}$ signal component is taken from the POWHEG-PYTHIA $t\bar{t}$ sample. The $t\bar{t}$ signal yields are normalized to match the data.

6.2.1 Unfolding

The reconstructed distributions are distorted from the true underlying distributions by the limited acceptance of our detector and by the resolution of reconstructed events. An unfolding procedure is used to correct the data for these two effects, in order to determine the $\Delta\phi_{l^+l^-}$ and $\cos(\theta_l^+) \times \cos(\theta_l^-)$ distributions, and resulting asymmetries, at parton-level. These distributions represent the differential cross-sections in the variables of interest, and are normalized to unity. The details of the unfolding procedure are described in Ref. [39].

The inclusive data sample (without $M_{t\bar{t}}$ cut) is used for the unfolded results, and any bias from acceptance effects is removed by the unfolding procedure. The background-subtracted and unfolded differential cross-sections for $\Delta\phi_{l^+l^-}$ and $\cos(\theta_l^+) \times \cos(\theta_l^-)$ are shown in Fig. 5. The data are compared to the predictions of the POWHEG-PYTHIA $t\bar{t}$ sample and to the NLO calculation from Ref.[34]. The asymmetries measured from the unfolded distributions are also parton-level quantities. The unfolded value of $A_{\Delta\phi}$ is $-0.097 \pm 0.015 \pm 0.036$ in data and -0.119 ± 0.0004 in the simulation. The unfolded value of A_{c1c2} is $-0.015 \pm 0.037 \pm 0.055$ in data and -0.063 ± 0.0004 in the simulation. The systematic uncertainties are from the sources described in Tab. 3.

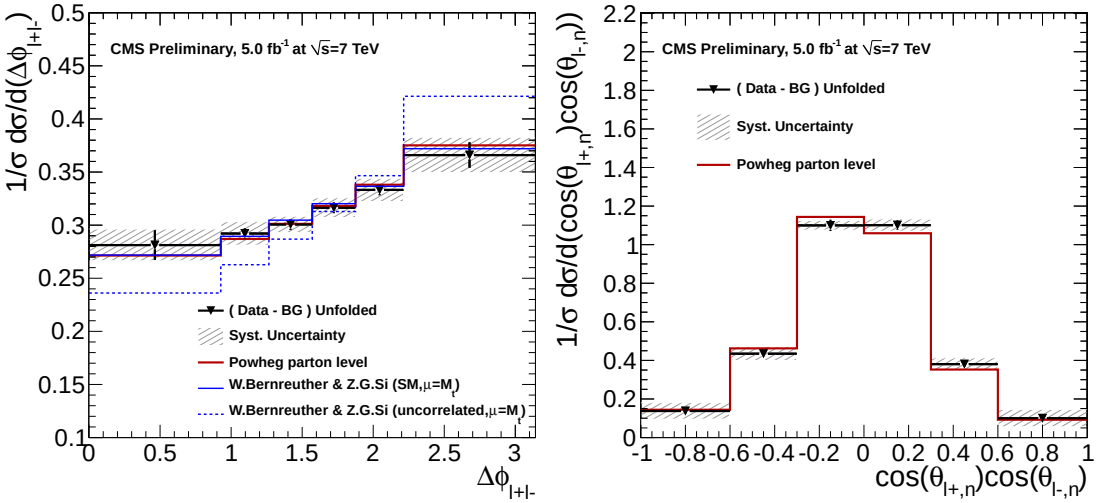

Figure 5: Background-subtracted and unfolded differential cross-sections for $\Delta\phi_{l^+l^-}$ and $\cos(\theta_l^+) \times \cos(\theta_l^-)$.

7 Conclusion

This note presents measurements related to the top spin correlation in $t\bar{t}$ dilepton final states (e^+e^-, $\mu^+\mu^-$ and $e^\pm\mu^\mp$). The spin correlation coefficient in the helicity basis is found to be $A_{hel.}^{meas.} = 0.24 \pm 0.02(\text{stat.}) \pm 0.08(\text{syst.})$ and comparable with the standard model prediction. The measurement is dominated by systematic uncertainties. A better understanding of the systematic effects related to theoretical predictions could yield a more precise measurement. The spin correlation is also investigated through asymmetry distributions, inclusively and at high $M_{t\bar{t}}$ at reconstruction level, and inclusively unfolded to parton level. The results are also in agreement with the SM predictions.

systematic	$A_{\Delta\phi}$	A_{c1c2}
statistic uncertainty	0.015	0.037
MC stat uncertainty	0.0004	0.0004
	experimental	
Lepton SF	0.0009	0.0002
Lepton energy scale	0.0009	0.0002
JES/JER	0.002	0.016
all backgrounds	0.002	0.010
PU	0.003	0.003
b-tagging	0.001	0.002
	$t\bar{t}$ modelling	
Fact. and renorm. scales	0.030	0.051
τ decay	0.016	0.002
top mass	0.002	0.005
PDF	0.009	0.001

Table 3: Uncertainty on the unfolded values of $A_{\Delta\phi}$ and A_{c1c2}

.

References

[1] Particle Data Group Collaboration, "Review of particle physics: ", *J. Phys.* **G37** (2010 and 2011 partial update for the 2012 edition) 075021, doi:10.1088/0954-3899/37/7A/075021.

[2] M. Beneke et al., "Top Quark Physics", arXiv:0003033.

[3] G. Mahlon and S. Parke, "Spin Correlation Effects in Top Quark Pair Production at the LHC", *Phys. Rev.* **D81** (2010) 074024, doi:10.1103/PhysRevD.81.074024.

[4] CDF Collaboration, "Measurement of $t\bar{t}$ Spin Correlation in $p\bar{p}$ Collisions Using the CDF II Detector at the Tevatron", *Phys. Rev.* **D83** (2011) 031104, doi:10.1103/PhysRevD.83.031104.

[5] D0 Collaboration, "Measurement of Spin Correlation in $t\bar{t}$ Production Using a Matrix Element Approach", *Phys. Rev. Lett.* **107** (2011) 032001, doi:10.1103/PhysRevLett.107.032001.

[6] D0 Collaboration, "Measurement of Spin Correlation in tt Production Using Dilepton Final States.", *Phys. Lett.* **B702** (2011) 16, doi:10.1016/j.physletb.2011.05.077.

[7] Atlas Collaboration, "Observation of spin correlation in ttbar events from pp collisions at sqrt(s) = 7 TeV using the ATLAS detector", arXiv:arXiv:1203.4081v1.

[8] "CMS technical design report, volume II: Physics performance", *J. Phys. G* **34** (2007) 995–1579, doi:10.1088/0954-3899/34/6/S01.

[9] S. Frixione and B. R. Webber, "Matching NLO QCD computations and parton shower simulations", *Journal of High Energy Physics* **2002** (2002), no. 06, 029.

[10] S. Frixione, P. Nason, and C. Oleari, "Matching NLO QCD computations with parton shower simulations: the POWHEG method", *JHEP* **11** (2007) 070, doi:10.1088/1126-6708/2007/11/070, arXiv:0709.2092.

[11] T. Sjöstrand, S. Mrenna, and P. Skands, "PYTHIA 6.4 physics and manual", *JHEP* **05** (2006) 026, arXiv:hep-ph/0603175.

[12] CMS Collaboration, "Comparison of the Fast Simulation of CMS with the first LHC data", (2011).

[13] J. Allison et al., "Geant4 developments and applications", *IEEE Trans. Nucl. Sci.* **53** (2006) 270, doi:10.1109/TNS.2006.869826.

[14] F. Maltoni and T. Stelzer, "MadEvent: Automatic event generation with MadGraph", *JHEP* **02** (2003) 027, arXiv:hep-ph/0208156.

[15] K. Melnikov and F. Petriello, "Electroweak gauge boson production at hadron colliders through $O(\alpha_s^2)$", *Phys. Rev.* **D74** (2006) 114017, doi:10.1103/PhysRevD.74.114017, arXiv:hep-ph/0609070.

[16] CMS Collaboration, "Measurement of the $t\bar{t}$ production cross section in the dilepton channel in pp collisions at $\sqrt{s} = 7$ TeV", *CMS Physics Analysis Summary* **CMS PAS TOP-11-005** (2011).

[17] CMS Collaboration, "Electron reconstruction and identification at $\sqrt{s}$=7 TeV", *CMS Physics Analysis Summary* **CMS-PAS-EGM-10-004** (2010).

[18] CMS Collaboration, "Performance of the muon identification in pp collisions at $\sqrt{s}$=7 TeV", *CMS Physics Analysis Summary* **CMS-PAS-EGM-10-004** (2010).

[19] CMS Collaboration, "Commissioning of the Particle-Flow reconstruction in Minimum-Bias and Jet Events from pp Collisions at 7 TeV", *CMS Physics Analysis Summary* **CMS-PAS-PFT-10-002** (2010).

[20] CMS Collaboration, "Measurement of the inclusive W and Z production cross sections in pp collisions at $\sqrt{s} = 7$ 7 TeV with the CMS experiment", *J. High Energy Phys* **10** (2011) 007, arXiv:1108.0566.

[21] M. Cacciari, G. P. Salam, and G. Soyez, "The anti-k_t jet clustering algorithm", *JHEP* **04** (2008) 063, doi:10.1088/1126-6708/2008/04/063, arXiv:0802.1189.

[22] M. Cacciari, G. Salam, and G. Soyez, "The Catchment Area of Jets", *JHEP* **04** (2008) 005, doi:10.1088/1126-6708/2008/04/05, arXiv:0802.1188.

[23] M. Cacciari and G. Salam, "Pileup subtraction using jet areas", *Phys. Lett.* **B659** (2008) 119, doi:10.1016/j.physletb.2007.09.077, arXiv:0707.1378.

[24] CMS Collaboration, "Jet Energy Corrections determination at 7 TeV", *CMS Physics Analysis Summary* **CMS-PAS-JME-10-010** (2010).

[25] CMS Collaboration, "b-Jet Identification in the CMS Experiment", *CMS Physics Analysis Summary* **CMS-PAS-BTV-11-004** (2012).

[26] CMS Collaboration, "Performance of the b-jet identification in CMS", *CMS Physics Analysis Summary* **CMS-PAS-BTV-11-001** (2011).

[27] CMS Collaboration, "CMS MET Performance in Events Containing Electroweak Bosons from pp Collisions at $\sqrt{s} = 7$ TeV", *CMS Physics Analysis Summary* **CMS-PAS-JME-10-005** (2010).

[28] D0 Collaboration, "Measurement of the $t\bar{t}$ production cross section in $p\bar{p}$ collisions at $\sqrt{s} =$ = 1.96-TeV using secondary vertex b tagging", *Phys.Rev.* **D74** (2006) 112004, arXiv:hep-ex/0611002.

[29] R. J. Barlow, "Event classification using weighting methods", *J.Comput.Phys.* **72** (1987) 202–219, doi:10.1016/0021-9991(87)90078-7.

[30] CMS Collaboration, "First Measurement of the cross section for Top-Quark Pair Production in Proton-Proton Collisions at sqrt(s)=7 TeV", *Phys. Lett.* **B695** (2011) 424, doi:10.1016/j.physletb.2010.11.058, arXiv:1010.5994.

[31] CMS Collaboration, "Measurement of the tt production cross section and the top quark mass in the dilepton channel in pp collisions at $\sqrt{s} = 7$ TeV", *JHEP* **1107** (2011) 049, arXiv:1105.5661.

[32] . http://www.hep.ucl.ac.uk/pdf4lhc/.

[33] RooFit, "The RooFit Toolkit for Data Modellin", doi:http://roofit.sourceforge.net/, arXiv:0306116.

[34] W. Bernreuther and Z.-G. Si, "Distributions and correlations for top quark pair production and decay at the Tevatron and LHC", *Nuc. Phys. B* **837** (2010) 90, arXiv:1003.3926.

[35] CDF Collaboration, "Forward-Backward Asymmetry in Top Quark Production in $p\bar{p}$ Collisions at $sqrts = 1.96$ TeV", *Phys.Rev.Lett.* **101** (2008) 202001, arXiv:0806.2472.

[36] D0 Collaboration, "First measurement of the forward-backward charge asymmetry in top quark pair production", *Phys.Rev.Lett.* **100** (2008) 142002, arXiv:0712.0851.

[37] D. Krohn, T. Liu, J. Shelton et al., "A Polarized View of the Top Asymmetry", *Phys.Rev.* **D84** (2011) 074034, doi:10.1103/PhysRevD.84.074034, arXiv:1105.3743.

[38] CMS Collaboration, "Measurement of the t t-bar production cross section and the top quark mass in the dilepton channel in pp collisions at sqrt(s) =7 TeV", *JHEP* **1107** (2011) 049, arXiv:1105.5661.

[39] CMS Collaboration, "Measurement of the top polarization in the dilepton channel", *CMS Physics Analysis Summary* **CMS-PAS-TOP-12-016** (2012).